SELF-SENSING AMB WITH COMPENSATION OF NON-LINEAR MAGNETIC EFFECTS

Alexandre Schammass
Laboratoire des Systèmes Robotiques, Swiss Federal Institute of Technology, 1015 Lausanne, Switzerland
alexandre.schammass@a3.epfl.ch

Raoul Herzog
Institut d'Automatisation Industrielle, Ecole d'Ingénieurs du Canton de Vaud, 1400 Yverdon-Les-Bains, Switzerland
raoul.herzog@eivd.ch

Philipp Bühler
MECOS Traxler AG, 8404 Winterthur, Switzerland
philipp.buehler@mecos.com

Hannes Bleuler
Laboratoire des Systèmes Robotiques, Swiss Federal Institute of Technology, 1015 Lausanne, Switzerland
hannes.bleuler@epfl.ch

ABSTRACT

This paper investigates the possibility to bring self-sensing active magnetic bearings to industrial application. A self-sensing active magnetic bearing is realized on an industrial prototype based on current amplitude modulation approach using a PWM amplifier. The performance limitations are investigated to identify the possible applications for this technology. This paper proposes a compensation of magnetic material permeability, which depends on the low frequency component of the current. The compensation is implemented using an approximated static permeability curve. Measurements were realized using a small industrial compressor prototype and applying the position estimator to one axis of one radial bearing. The estimated position was compared to the measured position obtained from a reference sensor.

INTRODUCTION

The concept of the self-sensing AMB is to eliminate the position sensors and estimate the position, by measuring the current in the electromagnetic coils. This represents not only a significant reduction of manufacturing costs, but also an increase in reliability and the compactness of the system.

Many self-sensing methods have been proposed in literature, however they are all very delicate to realize. Basically, there are two types of self-sensing AMBs: state estimation [12] and modulation [2], [4], [5], [8], [9], [11].

This paper investigates the realization of a self-sensing AMB suitable for industrial use. To accomplish this, a new approach to self-sensing AMB design is proposed and the performance limitations are investigated.

The self-sensing AMB is based on a modulation approach using the high frequency content of the current due to the PWM amplifier [10]. The position is estimated by measuring the coil current ripple. The position estimation is based on the bearing inductor model and includes the non-linearity of the magnetic material.

BEARING INDUCTOR MODEL

The modulation approach consists in obtaining the position information from the high frequency

components of the current. The position estimation is based on the bearing inductor model presented in this section. For simplicity, only one pole pair is modeled.

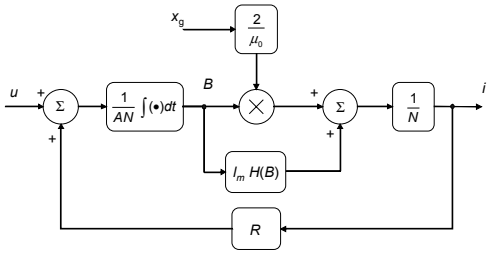

FIGURE 1: Simplified bearing inductor model: High bandwidth model.

A simplified bearing magnet model is shown in Figure 1. The model neglects the flux leakage, and the eddy current losses. It is also assumed that the behavior of the material is linear with constant relative permeability μ_r ($H(B) = B/\mu_r$) and saturation is neglected. A relationship among the current *i*, voltage *u* and gap x_g is obtained:

$$u = K\frac{d}{dt}\left(\frac{i}{2x_g + \frac{l_m}{\mu_r}}\right) + Ri \qquad (1)$$

where $K = \mu_0 N^2 A$ is the magnetic bearing constant, μ_0 is the magnetic permeability of free space, *N* represents the number of turns in the coil, *R* is the electric resistance, *A* is the cross section, l_m is the total core length.

To be used in the position estimation, the bearing inductor model considers only the first (fundamental) harmonic at the switching frequency of the voltage and the current, neglecting the other components (control and higher harmonics). The switching frequency is in the order of 20 times higher the control bandwidth.

The first harmonic signals are shifted to low frequencies by demodulation. The objective is to avoid unnecessary processing time due to the high frequency carrier. This can be an advantage for the model implementation in software.

To obtain the low bandwidth model, it is assumed that the voltage *u* and current *i* are filtered by an ideal band-pass in such a way that only the first harmonic is selected. The central frequency of the band-pass is set to the amplifier switching frequency ω_s. Under this condition, the inductive reactance $\omega_s L_0$ (where L_0 is the nominal inductance) is much larger than *R*, and therefore $Ri << u$. For the experimental setup, the ratio $R/(\omega_s L_0)$ is of the order of 0.2 %. Thus, equation (1) can be written:

$$i = \frac{1}{K}\left(2x_g + \frac{l_m}{\mu_r}\right)\int u dt \qquad (2)$$

The first harmonic of the PWM amplifier voltage can be expressed as $u = u_d \sin\omega_s t$, where u_d depends on the duty-cycle of the amplifier. Since the bandwidths of x_g and u_d are much smaller than the amplifier switching frequency ω_s, equation (2) can be written:

$$i = \frac{-1}{K\omega_s}\left(2x_g + \frac{l_m}{\mu_r}\right)u_d \cos\omega_s t \qquad (3)$$

In this way, the amplitude of the current *i* is obtained by demodulating the signal:

$$i_d = \frac{1}{K\omega_s}\left(2(x + x_0) + \frac{l_m}{\mu_r}\right)u_d \qquad (4)$$

where x_0 is the nominal air gap and *x* is the rotor position with respect to x_0.

Up to this point, the relative magnetic permeability μ_r was considered constant. However, this is not true because the material magnetization has a non-linear behavior and μ_r depends on the magnetic flux density *B*.

Many mathematical models including hysteresis have been proposed in the literature to account for the behavior of the material magnetization. The Preisach [3] and Jiles-Attherton [1] models are usually applied for determining hysteresis losses in magnetic systems e.g. transformers.

Here a simpler model is proposed taking into account saturation, but neglecting hysteresis. An ad hoc quadratic equation is approximated to the magnetization curve for a certain operating current range:

$$\frac{1}{\mu_r} \approx f_m(B) = a_{m2}B^2 + a_{m1}B + a_{m0} \qquad (5)$$

where a_{m2}, a_{m1} and a_{m0} are the coefficients of the polynomial. This quadratic approximation is substituted into equation (4):

$$i_d = (k_x x + k_{b2}B^2 + k_{b1}B + k_{b0})u_d \qquad (6)$$

where

$$k_x = \frac{-2}{K\omega_s},\ k_{b2} = \frac{l_m a_{m2}}{K\omega_s},\ k_{b1} = \frac{l_m a_{m1}}{K\omega_s} \text{ and } k_{b0} = \frac{l_m a_{m0}}{K\omega_s}.$$

The model described by equation (6) is shown in Figure 2. The magnetic flux density *B* for low frequencies can be calculated using the air gap x_g and the low frequency component of the current i_L:

$$B \approx \left[\frac{\mu_0 N}{2x_g} + \frac{L_s}{NA} \right] i_L \tag{7}$$

where L_s is the leakage inductance.

This model shows that high (i_d) and low frequency (i_L) components of the current are coupled due to the non-linearity of the magnetic material.

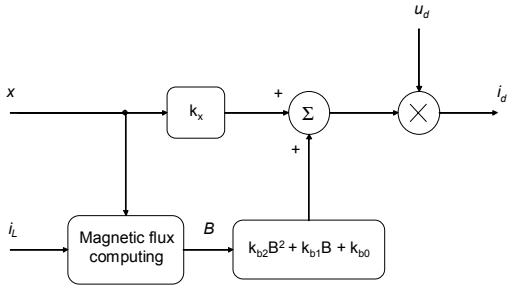

FIGURE 2: Simplified bearing inductor model: Low bandwidth model

To identify the parameters of the inductor model (k_x, k_{b0}, k_{b1}, k_{b2}), two simple experiments are performed. If the bias current is varied while the air gap is held constant ($x = 0$), it is possible to change only the magnetic flux density *B*. Measuring *x*, *i*, u_d and i_d, the parameters of the quadratic permeability function are determined using least squares.

The second step is to determine k_x. For this purpose, the bias current is kept constant and the position is varied by changing the value of the desired position.

POSITION ESTIMATION

Figure 3 shows the position estimation configuration. The voltage and current are measured and the estimation algorithm calculates the position of the rotor. The measured signals are demodulated and the resulting signals are processed at a low bandwidth.

The algorithm is based on the model inversion, which uses the low frequency component of the current i_L, the demodulated current i_d and the demodulated voltage u_d to estimate the position x_e. The position estimator can be divided into two parts: duty-cycle and permeability compensations.

Duty-Cycle Compensation

The first harmonics of the voltage and the current are obtained by filtering the signals with a band-pass (BPF). The filtering realized by the BPF and the low-pass of the demodulator limits the bandwidth of the estimated position. To obtain the amplitudes of the filtered current *i* and voltage *u*, both signals are demodulated.

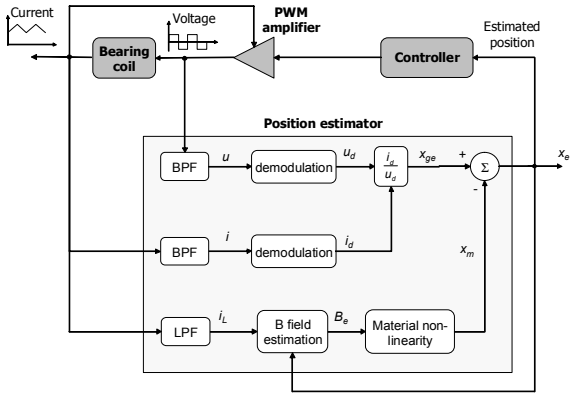

FIGURE 3: Estimation algorithm with permeability compensation

Neglecting the magnetic material, the demodulated current i_d basically depends on the product between the position *x* and the voltage component u_d (equation (4)). For this reason, the demodulated current is divided by the demodulated voltage.

$$x_{ge} = \frac{1}{k_x} \frac{i_d}{u_d} \tag{8}$$

It is assumed that the PWM amplifier setup guarantees that the demodulated voltage is never zero. This means that the division in equation (8) is well conditioned [10].

Permeability Compensation

As discussed before, the influence of the permeability cannot be neglected. For this reason, permeability changes are compensated as shown in Figure 3.

First, the low frequency part of the current i_L is obtained using a low-pass filter (LPF). The magnetic flux B_e can be calculated using equation (7). However, in this case the position *x* is substituted by the estimated position x_e (feedback). Approximating *x* to x_e and making $i = i_L$, the estimated magnetic flux B_e is written:

$$B_e \approx \left[\frac{\mu_0 N}{2(x_e + x_0)} + \frac{L_s}{NA} \right] i_L \tag{9}$$

In this case, the magnetic material function x_m is calculated from equation (6):

$$x_m = \frac{1}{k_x} (k_{b2} B_e^2 + k_{b1} B_e + k_{b0}) \tag{10}$$

As shown in Figure 3, the estimated position x_e is calculated:

$$x_e = x_{ge} - x_m = \frac{1}{k_x} \left(\frac{i_d}{u_d} - k_{b2} B_e^2 - k_{b1} B_e - k_{b0} \right) \tag{11}$$

EXPERIMENTAL RESULTS

Measurements were realized with the levitated rotor using the reference sensors. The estimated position was compared to the measured position obtained from the sensor. The quality of the estimated position is discussed in terms of static and dynamic performance. The system robustness is also evaluated from the control point of view.

Test Rig

Measurements were made using a small industrial compressor prototype shown in Figure 4. The system is composed of two radial bearings, one axial bearing and a short rotor with first bending mode at 1.5 kHz. The reference sensors used on the test rig were differential eddy current type. For the measurements, it was assumed that the reference sensor is more linear than the position estimator. The main characteristics of the system are the nominal air gap of 0.4 mm, and the maximum current of 1.2 A (bias current of 0.27 A). The rotor has a length of 235 mm, and a weight of 2.78 kg. The magnetic material used for the radial bearing is silicon steel.

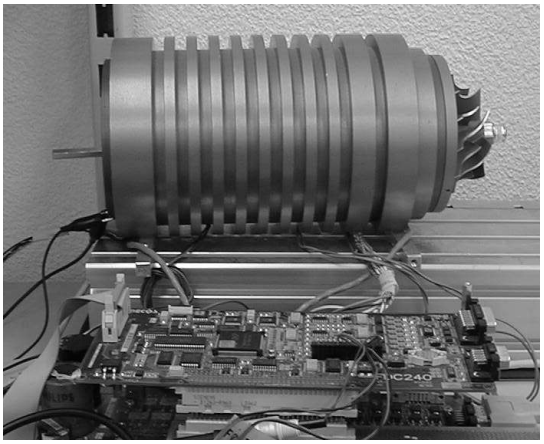

FIGURE 4: Experimental test rig.

The switching frequency of the PWM amplifier was 20 kHz. The position estimator was applied to one axis of one radial bearing (one DOF). To implement the algorithm, the band-pass filters and demodulators were built in an analog circuit. Each demodulator uses a second-order low-pass filter with a cutoff frequency of about 900 Hz. The compensation of duty-cycle and permeability, including the magnetic flux estimation were implemented in a DSP.

Before evaluating the position estimator, the parameters of the position estimator k_x, k_{b0}, k_{b1}, k_{b2} were identified. The values of these parameters are k_x $-1591.2\,\mathrm{m}^{-1}$, $k_{b2} = 0.2754\,\mathrm{T}^{-2}$, $k_{b1} = -0.1128$ T^{-1} and $k_{b0} = 0.9989$. To calculate the magnetic flux B, the following constants were used: $N = 560$, $x_0 = 0.4$ mm, $L_s = 18$ mH, $A = 166\ \mu\mathrm{m}^2$.

Static Performance of Estimation

To evaluate the linearity of the estimated position, the desired position is varied from -160 µm to 160 µm with bias current constant. Figure 5 shows the estimated position compared to the position measured by the sensor. For extreme positions (± 160 µm), the estimated position slightly deviates from the sensor signal.

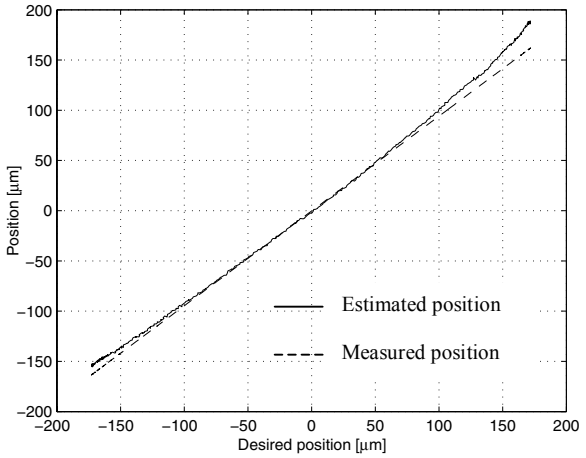

FIGURE 5: Estimator static performance compared to the position sensor for constant bias current.

Figure 6 shows the error between the estimated and measured positions ($x_e - x$), when the bias current was varied with the position constant. The error is plotted for different coil currents with and without permeability compensation. The results show that the permeability compensation can make the estimated position almost independent of static coil current.

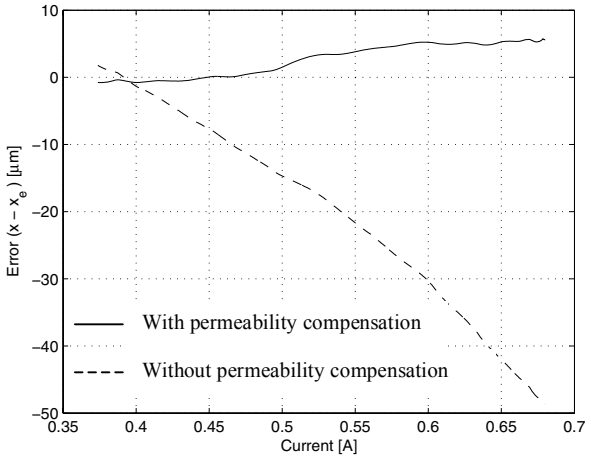

FIGURE 6: Estimator static performance compared to the position sensor for constant air gap.

The error observed for high currents is due to change of the magnetization curve. Further measurements have shown that the magnetization curve has some hysteresis, and therefore depends on its history. In this case, the quadratic curve parameters should be re-calibrated to minimize the error. The same experiment was repeated for other rotor positions (± 60 µm) with similar results.

Dynamic Performance of Estimation

Measurements were carried out in frequency domain to evaluate the dynamic performance of the position estimator. Although the self-sensing system is not linear, the frequency response was realized considering small position and current variations.

Figure 7 shows the frequency response of the estimated position with respect to the measured position $G_{ex}(\omega) = X_e(\omega)/X(\omega)$. The measurement shows the effect of the permeability compensation. This measurement was performed by adding a constant amplitude sinusoidal signal to the plant input.

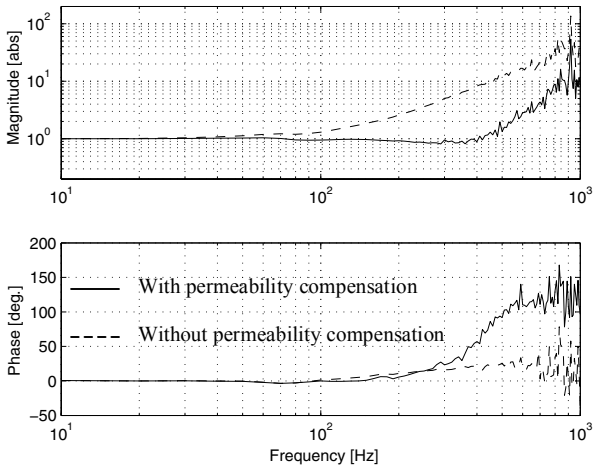

FIGURE 7: Frequency response of estimated position with respect to the sensor position. For both cases the duty-cycle is compensated

The ideal frequency response would have magnitude one and phase zero. The figure shows that the frequency response without permeability compensation is well behaved for low frequencies.

However, for frequencies above ca. 100 Hz, the phase remains small and the magnitude increases drastically.

Using the permeability compensation, the magnitude remains approximately one up to 400 Hz, and from this point gain and phase start to increase. Although frequency response is not ideal at high frequencies, the behavior of $G_{ex}(\omega)$ can be compensated by the controller.

Robustness

Robustness against loop gain variations is evaluated using the peak of the sensitivity function $\| S \|_\infty$. The robustness is poor for large values of $\| S \|_\infty$.

The sensitivity function was measured when the system was levitating with the estimated position. The position controller was tuned in order to minimize $\| S \|_\infty$ while keeping the dynamic stiffness in a reasonable range (rigid body mode around 100 Hz). The sensitivity function of the self-sensing configuration ($\| S \|_\infty \approx 3.5$) is good enough for most magnetic bearing applications. With the same controller for the self-sensing case, the rotor is levitated with position sensors. In this case, the measured value of $\| S \|_\infty$ is about 2.4.

A robustness comparison between the modulation and the state estimation approaches can be realized. The sensitivity function lower bound is derived in [7] for the linear magnetic bearing plant with unstable pole and non minimum-phase zero.

The sensitivity function lower bound is calculated for the test rig, simplifying the AMB system to one DOF. It is considered that displacement on the other radial bearing is small (the other radial bearing is substituted by a pivot). Using the transfer function between voltage and current presented in [2], the poles and zeros are determined for $m = 0.93$ kg (equivalent mass of the rotor), $k_s = Ki_0^2 / x_0^3 = 76.4$ kN/m (current-displacement constant), $L_0 = K/(2x_0) = 81.8$ mH, $L_s = 18$ mH and $R = 8.8\ \Omega$. The pole and zero on the right half-plane determine the $\| S \|_\infty$ lower bound at 4.94.

The results show that proposed self-sensing system, based on a modulation approach, can overcome the robustness limit imposed for linear time-invariant systems. This robustness improvement is possible due to the modulation approach [6].

CONCLUSION

This paper investigates the possibility to bring self-sensing active magnetic bearings to industrial application. A self-sensing active magnetic bearing is realized on an industrial prototype based on modulation approach using a PWM amplifier.

Experimental results show a good agreement between estimated and measured (sensor) positions for low frequencies. However, for high frequencies discrepancies appear and the estimated position amplitudes become larger than the measured position.

The reason for this behavior is investigated. Experimental results reveal that the estimated position is influenced by the current due to the magnetic material non-linearity.

This paper proposes a compensation of magnetic material permeability, which depends on the low frequency component of the current. The compensation is implemented using an approximated static permeability curve and almost eliminates the static current influence upon the estimated position. Moreover, the frequency response between the estimated and measured positions is improved.

In general, the results show that self-sensing active magnetic bearings can be used for a number of applications. However, the system has some limitations compared to the standard sensor case. The main reason for such limitations may be the magnetic material non-linearity. A model that better describes the magnetic permeability influence might attenuate these limitations.

AKNOWDEGEMENTS

The authors would like to thank the Kommission für Technologie und Innovation (KTI) for the financial support of this research project.

REFERENCES

1. D. C. Jiles, D. L. Atherton, *Theory of Ferromagnetic Hysteresis*, Journal of Magnetism and Magnetic Materials, v.61, n.1.
2. L. Kučera, *Zur Sensorlosen Magnetlagerung*, Diss. Nr. 12249, ETH Zurich, 1997.
3. I. D. Mayergoyz, *Mathematical Models of Hystheresis*, New York, NY, USA, Springer-Verlag, 1991.
4. T. Mizuno, T. Ishii, K. Araki, *Self-Sensing Magnetic Suspension Using Hysteresis Amplifiers*, in Proceedings of Fifth International Symposium on Magnetic Bearings, pp. 1133–1140, 1998.
5. D. T. Montie, E. H. Maslen, *Self-Sensing Results for a Magnetic Bearing*, in Proceedings of Sixth Symposium on Magnetic Suspension Technology, Turin, Italy, October, 2001.
6. D. T. Montie, *Performance Limitations and Self-Sensing Magnetic Bearings*, Ph.D. thesis, University of Virginia, USA, 2003.
7. N. Morse, R. Smith, B. Paden, J. Antaki, *Position Sensed and Self-sensing Magnetic Bearing Configurations and Associated Robustness Limitations*, in Proceedings of the 37th IEEE Conference on Decision and Control, pp. 2599–2604, Tampa, FL, USA, December, 1998.
8. M. D. Noh. *Self-Sensing Magnetic Bearing Driven by a Switching Power Amplifier*, Ph.D. thesis, University of Virginia, 1996.
9. Y. Okada, K. Matsuda, B. Nagai, *Sensorless Magnetic Levitation Control by Measuring the PWM Carrier Frequency Component*, in Proceedings of Third International Symposium on Magnetic Bearings, pp. 176–183, 1992.
10. A. Schammass, H. Bleuler, *Experimental Results on Self-Sensing AMB Using a Three-State PWM Amplifier*, in Proceedings of 8th International Symposium on Magnetic Bearings, p. 289–292, Mito, Japan, August, 2002.
11. N. Skricka, *Entwicklung eines sensorlosen aktiven Magnetlagers*, Diss., TU Darmstadt, Germany, 2004.
12. D. Vischer, H. Bleuler, *Self-sensing Magnetic Levitation*, IEEE Transactions on Magnetics, v.29, n.2, pp. 1276–1281, March, 1993.